Submitted to *Geophysical Research Letters*

Reservoir infill by hyperpycnal deltas over bedrock

Steven Y.J. Lai and H. Capart

Department of Civil Engineering and Hydrotech Research Institute, National Taiwan University,

No. 1, Sec. 4, Roosevelt Road, Taipei 10617, Taiwan

(Abstract)

We propose a simple morphodynamic theory of reservoir deltas prograding over bedrock under the influence of turbid underflows. The theory models the geomorphic actions of fluvial and hyperpycnal flows as diffusion processes, and treats bedrock-alluvial and river-lake transitions as moving internal boundaries. It yields self-similar analytical solutions for the co-evolving river and lake bed profiles, under different slope and influx conditions. These include a special case in which delta deposits are swept underwater to prograde into a subaqueous turbid pool. The theoretical predictions are in good agreement with laboratory experiments, and should help interpret and anticipate longitudinal sedimentation patterns in mountain reservoirs.

Keywords: reservoir sedimentation; turbidity current; river delta; diffusion equation.

1. Introduction

Reservoirs in the tectonically active mountains of Taiwan and Japan are subject to high rates of sediment infill [*Dadson et al.*, 2003; *Kashiwai*, 2005]. In converting from sediment supply to loss of effective storage capacity, one must discount sediment deposited on the delta foreset upstream of the reservoir [*Iwaizumi and Sidle*, 2007], as well as sediment transported to the deeper part of the reservoir below the minimum operational water level [*Umeda et al.*, 2006]. To estimate reservoir lifetime and evaluate countermeasures, the spatial distribution of sediment deposition must therefore be modeled. Currently, however, no interpretative or predictive model is available that embraces the variety of depositional patterns observed in practice [*Morris and Fan*, 1997]. Here we propose a simple theory of river and lake bed morphodynamics, applicable to reservoir deltas over bedrock subject to both fluvial and hyperpycnal influences. The theory extends the approach of *Lai and Capart* [2007], and draws from earlier work on fluvial, lacustrine and submarine diffusion [*Begin et al.*, 1981; *Kenyon and Turcotte*, 1985; *Jordan and Flemings*, 1991], as well as recent work on moving boundary problems [*Voller et al.*, 2004; *Capart et al.*, 2007]. Below we describe the proposed theory before testing it using experiments.

2. Theory

Motivated by the typical characteristics of mountain reservoirs in Taiwan and Japan (Fig.

36 1A), we consider a long, narrow lake created by damming a valley with bedrock sides and floor.
37 Neglecting width variations, we examine the long profile morphodynamics of the river and lake
38 beds. Alimented by the products of landsliding [*Hovius et al.*, 2000; *Iwaizumi and Sidle*, 2007],
39 supply-limited sediment transport drapes deltaic deposits over the bedrock floor both upstream
40 and downstream of the river-lake transition (Fig. 1B). Upstream, aggradation of the delta topset
41 raises the river bed, driving the headward migration of a transition between exposed bedrock and
42 alluvial cover [*Muto*, 2001]. Downstream, a delta foreset progrades into the reservoir. Bedload
43 transport along the foreset is driven by plunging underflows if the density of the turbid river
44 exceeds that of the lake (hyperpycnal case), or by gravitational avalanching otherwise (homo- or
45 hypopycnal case) [*Lai and Capart*, 2007]. In the hyperpycnal case, turbid currents flow along the
46 lake bottom before ponding at the deep end of the reservoir [*Toniolo et al.*, 2007], where they are
47 vented using bottom outlets. For simplicity, we assume that spilling and venting keep the
48 reservoir waterline and the internal density interface of the subaqueous turbid pool at constant
49 levels. We focus on the deposition of the coarser bedload fraction along the delta topset and
50 foreset, and neglect bed elevation changes due to fine sediment settling out of the fluvial and
51 hyperpycnal flows. Bottom set beds are thus excluded from consideration.

52 We assume that the bedrock river has initial profile $z_0(x) = -S_0 x$, where $S_0 = \tan\theta$ is the
53 bedrock inclination, and spatial coordinate x is measured in the direction of the valley axis. A

steady river flow rate Q discharges into the reservoir maintained at constant level $z = 0$. Starting from bare bedrock, at time $t = 0$, the upstream reach of the river is supplied with bedload at steady volumetric rate I. As this flux is lower than the transport capacity of the bedrock river (supply-limited conditions), sediment will not deposit before reaching the aggrading delta. The deltaic profile evolution is subject to the Exner equation

$$\frac{\partial z}{\partial t} + \frac{\partial j}{\partial x} = 0 \tag{1}$$

where $z(x,t)$ is the bed profile elevation above base level, and $j(x,t)$ is the bedload transport rate, taken as a volumetric flux of bed material (sediment + pore space) per unit width. Bedrock and angle-of-stability constraints require that

$$z(x,t) \geq z_0(x), \qquad \left|\frac{\partial z}{\partial x}\right| \leq R, \tag{2}$$

where $R = \tan\varphi$ is the slope beyond which avalanching occurs. Except where avalanching takes place, we assume that the bedload transport rate j is governed by the modified diffusive relation

$$j(x,t) = D(S - S_{\min}), \tag{3}$$

where D is the diffusivity, $S = -\partial z / \partial x$ is the local bed inclination, $S_{\min}$ is a minimum inclination required for bedload transport, and it is implied that $S > S_{\min}$. Alternatively, this relation can be interpreted as a two-term approximation to a more complicated empirical or predictive bedload transport law [*Hsu and Capart*, 2008]. We found in earlier work [*Lai and Capart*, 2007] that Eq. (3) can be applied to both the topset and foreset of hyperpycnal deltas

72 provided that different values D_1, D_2, for the diffusivity, and $S_{\min,1}$, $S_{\min,2}$ for the minimum
73 inclination are considered for fluvial and hyperpycnal bedload.

74 For deltas over bedrock (Fig. 1B), let $s^{(1)}(t)$, $s^{(2)}(t)$ denote the positions of the
75 bedrock-alluvial and river-lake (or topset-foreset) transitions. Upon substituting Eq. (3) in Eq. (1),
76 we obtain the two diffusion equations

77 $$\frac{\partial z_1}{\partial t} - D_1 \frac{\partial^2 z_1}{\partial x^2} = 0, \qquad s^{(1)}(t) < x < s^{(2)}(t), \tag{4}$$

78 $$\frac{\partial z_2}{\partial t} - D_2 \frac{\partial^2 z_2}{\partial x^2} = 0, \qquad s^{(2)}(t) < x, \tag{5}$$

79 where D_1 and D_2 are the subaerial and subaqueous diffusivities ($D_1 > D_2$), and $z_1(x, t)$ and $z_2(x, t)$
80 are the topset and foreset profiles (Fig. 1B). As in *Voller et al.* [2004] and *Capart et al.* [2007],
81 the two moving boundaries $s^{(1)}(t)$, $s^{(2)}(t)$ migrate according to

82 $$s^{(\beta)}(t) = \lambda^{(\beta)} \sqrt{D_1 t}, \qquad \beta = 1, 2, \tag{6}$$

83 where $\lambda^{(1)}$ and $\lambda^{(2)}$ are dimensionless constants governing the time-evolving positions of the
84 delta boundaries. Analytical solutions for the bed profiles $z_\alpha(x,t)$, $\alpha = 1, 2$, then take the
85 self-similar form [for a derivation, see *Capart et al.*, 2007]

86 $$\frac{z_\alpha}{\sqrt{D_\alpha t}} = -A_\alpha \frac{x}{\sqrt{D_\alpha t}} + B_\alpha \,\mathrm{ierfc}\left(\frac{x}{2\sqrt{D_\alpha t}} \right) \tag{7}$$

87 where the special function ierfc is the first integral of the complementary error function. The
88 coefficients A_1, B_1, for the topset, A_2, B_2, for the foreset, and $\lambda^{(1)}$, $\lambda^{(2)}$, for the moving

89 boundaries, are obtained from the internal and external boundary conditions. These include, at the
90 bedrock-alluvial and river-lake transitions, the prescribed elevations

91 $$z_1(s^{(1)}(t),t) = -S_0 s^{(1)}(t), \qquad z_1(s^{(2)}(t),t) = z_2(s^{(2)}(t),t) = 0, \tag{8}$$

92 as well as continuity of the bedload fluxes

93 $$j_1(s^{(1)}(t),t) = I, \qquad j_1(s^{(2)}(t),t) = j_2(s^{(2)}(t),t). \tag{9}$$

94 where $j_\alpha = D_\alpha(-\partial z_\alpha / \partial x - S_{\min,\alpha})$, $\alpha = 1, 2$. Two boundary conditions must be applied at each
95 transition because their migration histories are part of the problem to be solved.

96 Two additional cases can be addressed by slightly modifying the above model. For
97 homopycnal conditions, the subaqueous diffusivity D_2 becomes equal to zero, and avalanching
98 takes over instead of underflow-driven bedload along the delta front. Equations and boundary
99 conditions for the river bed are the same as before, save for the sediment flux condition at the
100 shoreline which becomes [*Voller et al.*, 2004; *Capart et al.*, 2007]

101 $$j_1(s^{(2)}(t),t) = \frac{RS_0(\lambda^{(2)})^2}{2(R - S_0)}. \tag{10}$$

102 Finally, if the bedload influx I is weak compared to the transport capacity of the turbid underflow,
103 $I < D_2(S_0 - S_{\min,2})$, deltaic deposits can be completely swept into the lake. Bedload then
104 bypasses the river-lake transition to form a subaqueous delta prograding into the turbid pool.
105 Hyperpycnal flow drives transport along the delta topset, and the base level ($z = 0$) must be
106 switched from the waterline to the internal density interface, under which avalanching occurs.

107

108 **3. Experiments**

109 We use small-scale laboratory experiments to test the ability of the theory to model different
110 types of deltas over bedrock. Experiments are conducted in a narrow flume (length = 1 m; width
111 = 1 cm), constructed with transparent parallel walls and a rough, rigid floor. Downstream, the
112 flume is fitted with weirs to control the lake waterline and subaqueous density interface.
113 Upstream, a constant head tank supplies the river discharge, and a silo-fed conveyor belt supplies
114 bedload sediment. For the river discharge, either freshwater (ρ = 1.0 g ml^{-1}) or brine (ρ = 1.2
115 g ml^{-1}) are used to obtain homopycnal or hyperpycnal inflows into the freshwater lake. For the
116 bedload sediment, sand of median diameter d_{50} = 0.17 mm, coefficient of uniformity d_{60} / d_{10} =
117 2.3, and angle of repose φ = 36º is chosen. Green fluorescent dye is added to the brine to
118 visualize underflows, and black ash is sprinkled at repeated intervals to visualize the stratigraphy
119 of the deposits. Time-lapse photography is used to monitor the evolution of the river and lake
120 beds, with photos acquired at intervals of 5 sec. Bed elevation measurements are obtained by
121 digitizing profiles from the timelapse photographs and translating them to metric coordinates
122 using a calibrated linear conformal transformation.

123 We present on Fig. 2 four experiments designed to document the effects of inflow density
124 (homopycnal versus hyperpycnal), inclination (moderate to steep), and bedload supply (high to

125 low) on the morphology of deltas over bedrock. To gauge the influence of inflow density,
126 experiments A and B (Fig. 2A,B) show deltaic morphologies resulting from homopycnal and
127 hyperpycnal river inflows, respectively, over bedrock floors of moderate inclination (θ = 10º).
128 Experiments with homopycnal deltas over bedrock were reported earlier [*Muto*, 2001], hence
129 experiment A serves as a baseline case. To examine the effect of inclination, experiment C is
130 conducted under the same hyperpycnal conditions as experiment B, with the steepness of the
131 bedrock floor increased twofold to θ = 20º. Experiment D shows what happens under the same
132 conditions when the bedload supply is decreased by a factor of 5, and the hyperpycnal current
133 ponds into a subaqueous pool at the downstream end of the flume. To facilitate comparison, all
134 tests are performed under the same river discharge, held steady at volumetric flow rate per unit
135 width Q = 80.6 mm^2 s^{-1}. For small scale experiments, transport relations are expected to take the
136 following power law form [see e.g. *Swenson and Muto*, 2007; *Hsu and Capart*, 2008]

137 $$j(x,t) = aQS^b \,, \tag{11}$$

138 instead of the simpler Eq. (3), where a and b are dimensionless empirical coefficients. To
139 translate from Eq. (11) to Eq. (3), we use a two term Taylor expansion around a reference slope
140 S_{ref}. We set $S_{\mathrm{ref}} = S_{\mathrm{eq}}$ for fluvial transport and $S_{\mathrm{ref}} = \frac{1}{2}(S_0 + S_{\mathrm{eq}})$ for hyperpycnal transport,
141 where $S_{\mathrm{eq}} = (I/(aQ))^{1/b}$ is the slope that equilibrates the sediment influx I. Different values of
142 coefficient a apply to fluvial and hyperpycnal transport, but a common exponent b is used.

4. Experimental results

Depicted by the photographs of Fig. 2 are the mature deltaic deposits formed at late stages of the four experiments, when the shallow fluvial and hyperpycnal flows (from left to right) are still active. Experiment A (Fig. 2A), performed under homopycnal conditions, leads to a classical Gilbert delta, with a topset of mild inclination, a steep foreset inclined at the angle of repose (φ = 36º), and sharp slope breaks at the shoreline and foreset toe. Experiment B (Fig. 2B), by contrast, shows the influence of hyperpycnal conditions (ratio of river density to lake density = 1.2). Under the influence of the gravity underflow (thin green layer), the foreset becomes more elongated, reduces its maximum inclination (to well below the angle of repose), and adopts a concave upwards curvature allowing the foreset toe to connect smoothly with the lake bottom. Unlike the subaqueous foresets, the subaerial topsets of experiments A and B are similar to each other in shape and inclination. In both cases, the topset terminates upstream at a well-defined transition between exposed bedrock and alluvial cover, which migrates headward as the delta grows.

Experiment C (Fig. 2C) provides further information about the response of the bedrock-alluvial transition. For this steeper inclination (θ = 20º), the hyperpycnal flow drives a greater proportion of the river bedload into the lake. The delta foreset becomes highly elongated, leaving only a short topset between the bedrock-alluvial transition and the shoreline. Experiment

161 D (Fig. 2D), finally, confirms that it is possible for hyperpycnal flows over bedrock to drive the
162 entire river bedload into the lake, provided that the bedload supply is sufficiently low. Upon
163 reducing the bedload supply by a factor of 5 (compared to experiment C), the hyperpycnal
164 underflow is able to drive the entire river bedload flux through the shoreline, making the
165 subaerial delta disappear. A subaqueous delta forms instead, prograding into the turbid pool.
166 Despite their different environments, the subaqueous delta of experiment A is quite similar in
167 morphology to the subaerial delta of experiment D. Both feature short, straight foresets inclined
168 at the angle of repose, and long topsets of mild concave upwards curvature. Where they differ is
169 in their topset inclination, much steeper in the subaqueous case D than in the subaerial case A.
170 Cases C and D underscore that, over the same bedrock inclination, it is possible for lake deposits
171 to exhibit very different depositional patterns. Dependent on the bedload influx (strong versus
172 weak), downstream (case C) or upstream tapering (case D) of the underwater deposits is observed,
173 flipping the direction in which deposits become gradually thinner.
174
175 **5. Comparison and discussion**
176 Measured river and lake bed profiles are plotted in Fig. 3. A consequence of the theory is
177 that, for each experiment, delta profiles acquired at different times should collapse together when
178 plotted in normalized coordinates $x/\sqrt{It}$, $z/\sqrt{It}$. This geometrical self-similarity is verified to

179 a very good approximation by the experimental data (dots obtained at four different times t_1 to
180 t_4 collapse together). The delta morphology is thus independent of the time of observation, and
181 delta growth produces an internal stratigraphy composed of nested profiles representing
182 homothetic replicas of each other. This explains, on Fig. 2, the self-similar stacking of trapped
183 ash layers in the experimental deposits. Because of self-similarity, moreover, the sediment flux *j*
184 at any location *s* can be estimated from each measured profile $z(x,t)$ using the formula

185 $$j(s,t) = I + \frac{(z(s,t) - z_0(s))s}{2t} - \frac{1}{t}\int_{-\infty}^{s} (z(x,t) - z_0(x))dx\,, \qquad (12)$$

186 and the bed inclination *S* at the same location can be estimated by differencing. We use the
187 resulting empirical relationship $j(S)$ to calibrate the transport coefficients *a* and *b* in Eq. (11).
188 The resulting values are $a = 130$ for fluvial transport, $a = 0.65$ for hyperpycnal transport, and $b =$
189 3.5 for the exponent. Using the same calibrated values for all cases, the theoretical profiles
190 plotted in Fig. 3A-D are found to be in close agreement with the measured data. The bed shapes
191 and elevations are well predicted, with only slight errors in phase for the positions of the delta
192 fronts. Most important, the theory is able to reproduce the wide behavioral range of the
193 experimental deltas. This range includes the production of straight and curved foresets (A versus
194 B), contrasted ratios of foreset to topset length (B versus C), and the formation of underwater
195 deposits of opposite tapers (C versus D). The theory may therefore help make sense of the very
196 different depositional patterns that have been documented in mountain reservoirs.

197 In Taiwan, a Gilbert-type delta similar to case A has led to the recent infill of the small
198 Ronghua reservoir, upstream of the large Shimen reservoir [*Capart et al.*, 2007]. In the Ronghua
199 case, river inflow is highly turbid during flood [*Lee et al.*, 2006], yet homopycnal conditions
200 prevail because the small reservoir rapidly becomes turbid itself, blurring the density contrast
201 between inflow and lake. The large Shihmen reservoir, on the other hand, features deposits
202 similar to case D, which become thicker rather than thinner going into the lake. During and after
203 flood, the reservoir is known to host a long-lasting turbid pool at its deep end [*Hsu*, 2006], and
204 receives very little bedload because the latter is intercepted by the Ronghua reservoir.
205 Well-known hyperpycnal deltas having morphologies matching cases B and C are the deltas of
206 the Upper Rhine at Lake Constance [*Hinderer*, 2001], and the Colorado River at Lake Mead
207 [*Graf*, 1971; *Kostic and Parker*, 2003]. The Upper Rhine delta, in a valley of moderate
208 inclination, exhibits a very long topset and a short foreset, whereas the Colorado river delta, in a
209 valley of steeper inclination, features a short topset and an elongated foreset. The same contrast is
210 observed in two different arms of Lake Billy Chinook, Oregon [*O'Connor et al.*, 2003].
211
212 **6. Conclusion**
213 In this work, we proposed and tested a theory of reservoir infill by delta progradation over
214 bedrock. The theory describes the joint evolution of the river and lake beds under fluvial and

215 hyperpycnal transport, subject to limited sediment supply. Unlike other recent models of deltaic
216 sedimentation [e.g. *Kostic and Parker*, 2003; *Gerber et al.*, 2008], our description is sufficiently
217 simple to be tractable analytically. Nevertheless, it can reproduce the diverse sedimentation
218 patterns generated in our experiments. Similar to distributions encountered in actual reservoirs,
219 these patterns include lacustrine deposits of varied curvatures, lengths, and tapers. The theory
220 further predicts, and experiments confirm, that weak bedload supply to the bedrock river can be
221 entirely driven into the lake by hyperpycnal underflows. In spite of these encouraging results,
222 certain important features of actual reservoir processes fall outside the scope of the theory, and
223 will require further work. These include possibly significant bed changes due to the settling of
224 fine sediment out of suspension, fluctuating reservoir or turbid pool levels, and the effects of
225 more complex bathymetry and reservoir stratification.
226
227 **Acknowledgments**
228 Financial support for this work was provided by the National Science Council and by the Tsung
229 Cho Chang Educational Foundation, Taiwan. At National Taiwan University, J.P.C. Hsu, C.Y.
230 Hao, and W. Wang contributed to exploratory experiments with homopycnal deltas, and F. C. Wu,
231 D. L. Young, and L. S. Teng offered valuable feedback.
232

233 **References**

234 Begin, Z.B., D.F. Meyer, and S.A. Schumm (1981), Development of longitudinal profiles of
235 alluvial channels in response to base level lowering, *Earth Surf. Processes Landforms*, *6*,
236 49–68.

237 Capart, H., M. Bellal, and D.L. Young (2007), Self-similar evolution of semi-infinite alluvial
238 channels with moving boundaries, *J. Sediment. Res.*, *77*, 13–22.

239 Dadson, S.J., N. Hovius, H. Chen, W. B. Dade, M. -L. Hsieh, S.D. Willett, J.-C. Hu, M.-J. Horng,
240 M.-C. Chen, C.P. Stark, D. Lague and J.-C. Lin (2003), Links between erosion, runoff
241 variability and seismicity in the Taiwan orogen, *Nature*, *426*, 648–651.

242 Gerber, T.P., L.F. Pratson, M.A. Wolinsky, R. Steel, J. Mohr, J.B. Swenson, and C. Paola (2008),
243 Clinoform progradation by turbidity currents: Modeling and experiments, *J. Sediment. Res.*,
244 *78*, 220–238.

245 Graf, W. H. (1971), Hydraulics of Sediment Transport, McGraw-Hill, New York.

246 Hinderer, M. (2001), Late Quaternary denudation of the Alps, valley and lake fillings and modern
247 river loads, *Geodin. Acta*, *14*, 231–263.

248 Hovius, N., C.P. Stark, H.T. Chu, and J.C. Lin (2000), Supply and removal of sediment in a
249 landslide-dominated mountain belt: Central Range, Taiwan, *J. Geol.*, *108*, 73–89.

250 Hsu, S.T. (2006), Problems encountered in Shihmen reservoir and the improvement plans,

Proceedings of the 1st Taiwan-Japan Workshop on Flood Hazard Mitigation, Taipei, Taiwan.

Hsu, J.P.C., and H. Capart (2008), Onset and growth of tributary-dammed lakes, *Water Resources Research*, in press.

Imaizumi, F., and R.C. Sidle (2007), Linkage of sediment supply and transport processes in Miyagawa Dam catchment, Japan, *J. Geophys. Res.*, *112*, F03012.

Jordan, T.E., and P.B. Flemings (1991), Large-scale stratigraphic architecture, eustatic variation, and unsteady tectonism: A theoretical evaluation, *J. Geophys. Res.*, *96*, 6681–6699.

Kashiwai, J. (2005), Reservoir Sedimentation and Sediment Management in Japan, *Technical Memorandum of Public Works Research Institute*, *3957*, 240–250.

Kenyon, P.M., and D.L. Turcotte (1985), Morphology of a delta prograding by bulk sediment transport, *Geol. Soc. Am. Bull.*, *96*, 1457–1465.

Kostic, S., and G. Parker (2003), Progradational sand-mud deltas in lakes and reservoirs. Part 1. Theory and numerical modeling, *J. Hydraul. Res.*, *41*, 127–140.

Lai, S.Y.J., and H. Capart (2007), Two-diffusion description of hyperpycnal deltas, *J. Geophys. Res.*, *112*, F03005.

Lee, H.-Y., Y.-T. Lin, and Y.-J. Chiu (2006), Quantitative estimation of reservoir sedimentation from three typhoon events, *J. Hydraul. Eng.*, *11*, 362–370.

Morris, G., and J. Fan (1997), *Reservoir sedimentation handbook*, McGraw-Hill, New York.

269 Muto, T., (2001), Shoreline autoretreat substantiated in flume experiments, *J. Sedim. Res.*, *71*,
270 246–254.
271 O'Connor, J.E., G.E. Grant, and T.L. Haluska (2003), Overview of geology, hydrology,
272 geomorphology, and sediment budget of the Deschutes River Basin, Oregon, in J.E.
273 O'Connor and G.E. Grant (eds), A Peculiar River, *Water Science and Application*, *7*, 7–30.
274 Swenson, J.B., and T. Muto (2007), Response of coastal plain rivers to falling relative sea-level:
275 allogenic controls on the aggradational phase, *Sedimentology*, *54*, 207–221.
276 Toniolo, H., G. Parker, and V. Voller (2007), Role of ponded turbidity currents in reservoir trap
277 efficiency, *J. Hydraul. Eng.*, *133*, 579–595.
278 Umeda, M., K. Yokoyama, and T. Ishikawa (2006), Observation and Simulation of Floodwater
279 Intrusion and Sedimentation in the Shichikashuku Reservoir, *J. Hydraul. Eng.*, *132*, 881–891.
280 Voller, V.R., J.B. Swenson, and C. Paola (2004), An analytical solution for a Stefan problem
281 with variable latent heat, *Int. J. Heat Mass Transfer*, *47*, 5387–5390.

Figure captions

Figure 1. Hyperpycnal deltas prograding over bedrock into narrow reservoirs: (a) Wanda Reservoir, Central Taiwan (photo by H. Capart); (b) Schematic long profile of a generic mountain reservoir [adapted from *Morris and Fan*, 1997; *Lai and Capart*, 2007].

Figure 2. Experimental deltas over bedrock: (a) homopycnal delta (bedload influx I = 5.7 $\mathrm{mm^2\ s^{-1}}$, bedrock inclination $\theta = 10°$); (b) hyperpycnal delta (I = 5.2 $\mathrm{mm^2\ s^{-1}}$, $\theta = 10°$); (c) hyperpycnal delta over steeper bedrock slope (I = 5.2 $\mathrm{mm^2\ s^{-1}}$, $\theta = 20°$); (d) hyperpycnal delta supplied with lower rate of bedload influx (I = 0.94 $\mathrm{mm^2\ s^{-1}}$, $\theta = 20°$).

Figure 3. Comparison of measured (dots) and theoretical profiles (lines) for the experimental deltas of Fig. 2. Data points colored red, green, blue, and orange denote delta profiles measured at evenly spaced time t_1 to t_4. Normalized coordinates are used to demonstrate self-similarity.

Figures

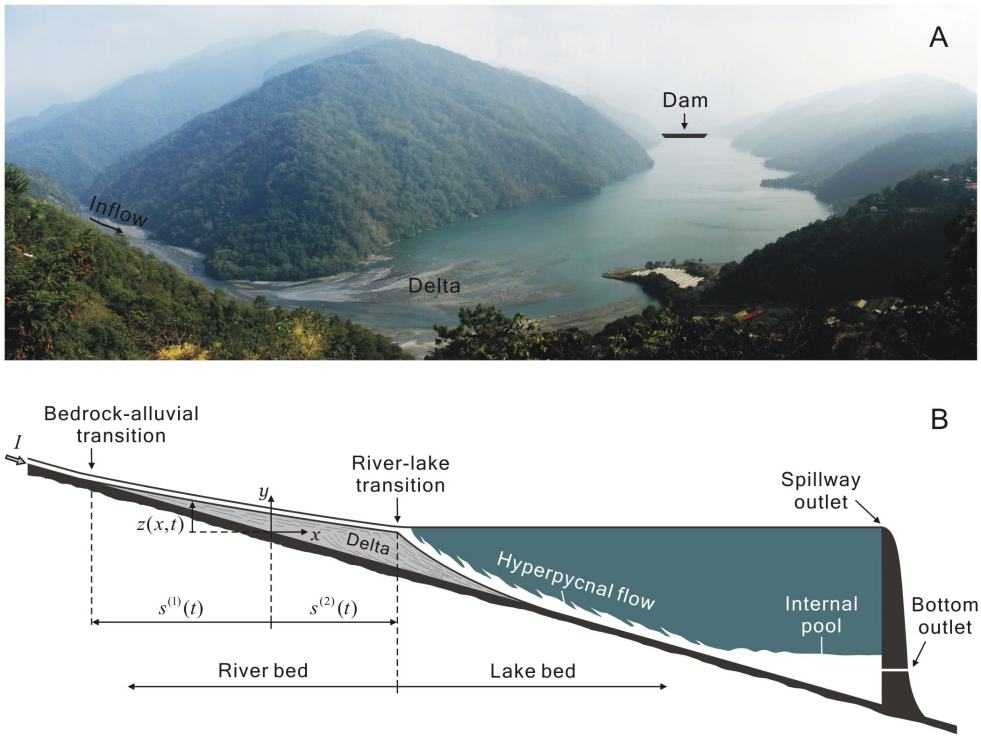

Figure 1. Hyperpycnal deltas prograding over bedrock into narrow reservoirs: (a) Wanda Reservoir, Central Taiwan (photo by H. Capart); (b) Schematic long profile of a generic mountain reservoir [adapted from *Morris and Fan*, 1997; *Lai and Capart*, 2007].

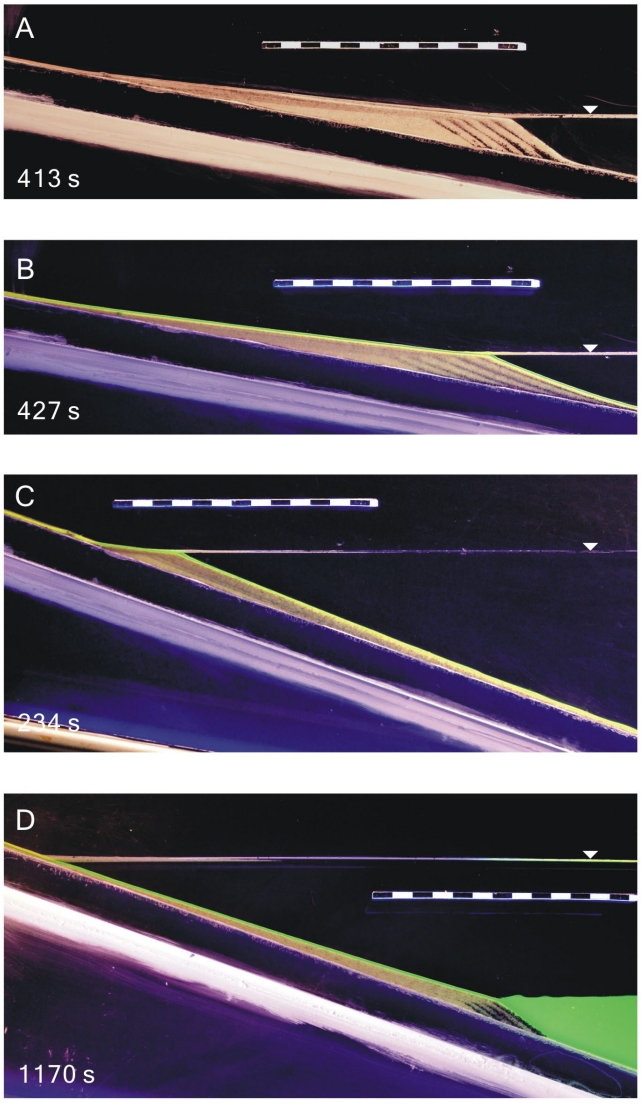

300

301 **Figure 2.** Experimental deltas over bedrock: (a) homopycnal delta (bedload influx I = 5.7

302 mm^2 s^{-1}, bedrock inclination $\theta = 10°$); (b) hyperpycnal delta (I = 5.2 mm^2 s^{-1}, $\theta = 10°$); (c)

303 hyperpycnal delta over steeper bedrock slope (I = 5.2 mm^2 s^{-1}, $\theta = 20°$); (d) hyperpycnal delta

304 supplied with lower rate of bedload influx (I = 0.94 mm^2 s^{-1}, $\theta = 20°$).

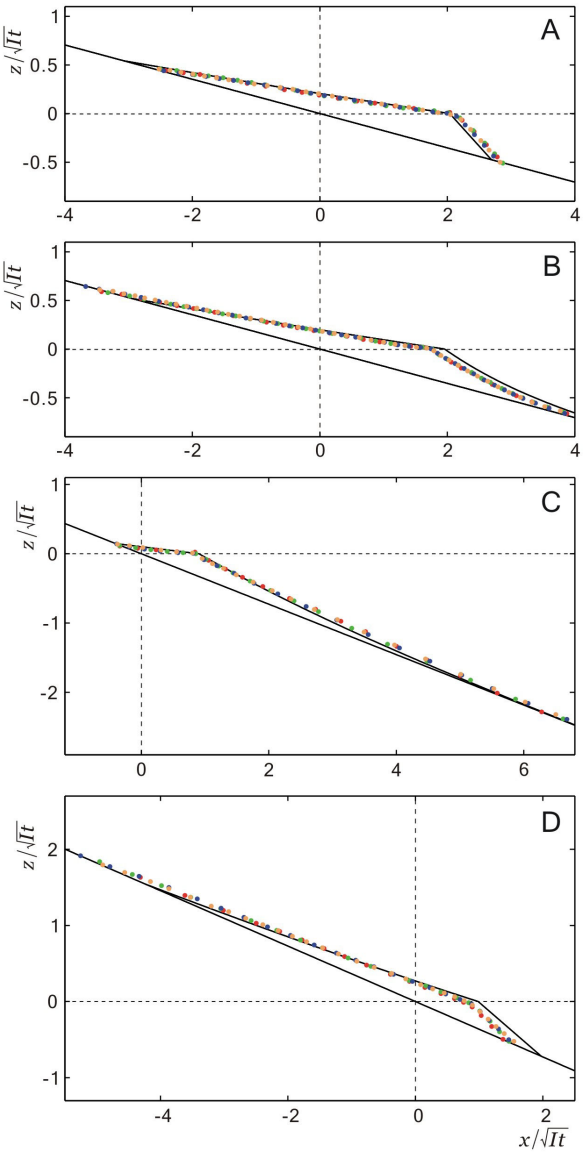

Figure 3. Comparison of measured (dots) and theoretical profiles (lines) for the experimental deltas of Fig. 2. Data points colored red, green, blue, and orange denote delta profiles measured at evenly spaced time t_1 to t_4. Normalized coordinates are used to demonstrate self-similarity.